Multifold Increases in Turing Pattern Wavelength in the Chlorine Dioxide-Iodine-Malonic Acid Reaction-Diffusion System

Delora K. Gaskins, Emily E. Pruc, Irving R. Epstein, and Milos Dolnik
Department of Chemistry, Brandeis University, Waltham, Massachusetts 02453, USA
(Received 16 March 2016; revised manuscript received 8 June 2016; published 29 July 2016)

Turing patterns in the chlorine dioxide-iodine-malonic acid reaction were modified through additions of sodium halide salt solutions. The range of wavelengths obtained is several times larger than in the previously reported literature. Pattern wavelength was observed to significantly increase with sodium bromide or sodium chloride. A transition to a uniform state was found at high halide concentrations. The observed experimental results are qualitatively well reproduced in numerical simulations with the Lengyel-Epstein model with an additional chemically realistic kinetic term to account for the added halide and an adjustment of the activator diffusion rate to allow for interhalogen formation.

DOI: 10.1103/PhysRevLett.117.056001

Pattern formation is diverse and ubiquitous. There are several types of instabilities capable of generating patterns. The Turing instability gives rise to patterns through destabilization of a uniform steady state. Such Turing patterns are periodic in space and stationary in time and have a characteristic wavelength that is independent of the size of the system. The Turing instability has been used to explain pattern formation in a variety of biological and ecological systems, including patterns on butterflies and fish [1–3], mouse digit formation [4], and plant patterns in arid and semiarid ecosystems [5,6].

Changes in morphology and wavelength of a pattern in a system may indicate and lead to significant consequences for the system. In arid ecosystems, changes in pattern morphology and wavelength may serve as warning signs prior to desertification [7,8]. Extinction of species through loss of habitat due to habitat fragmentation can arise when biomass patterns become less connected as a result of changes in pattern morphology and wavelength. Habitat fragmentation has been argued to be one of the most important threats to global biodiversity [9,10]. The evolutionary fitness of patterned animals such as guppies and zebras has been proposed to depend on the wavelength of the pattern on their skins [11,12].

In this Letter, we induce wavelength changes in Turing patterns found in the chlorine dioxide-iodine-malonic acid (CDIMA) reaction [13]. The CDIMA reaction, which is related to the chlorite-iodide-malonic acid (CIMA) reaction, in which Turing patterns were first experimentally observed [14], is the prototypical reaction for the study of Turing patterns in reaction-diffusion systems [15]. The chlorinated species act as an inhibitor and the iodine-containing species serve as an activator in this system. The requisite difference between the diffusion coefficients of the activator and inhibitor for Turing patterns is achieved through complexation with an indicator, which slows the effective diffusion of the iodide species.

Prior work with these systems shows that the wavelength of the pattern is nearly independent of the feed concentration of the input reagents—with the exception of $[ClO_2]$. The wavelength of the pattern increases as the ClO_2 concentration is decreased [16]. Other factors that can alter the wavelength of the pattern by affecting diffusion include the identity and concentration of the complexing agent of the iodide [17] and the gel identity and density [18]. Slowing the rate at which a pattern can regrow at the edge of a steady state-pattern interface also allows for longer pattern wavelengths to be achieved [19]. The longest wavelength obtained through perturbation of CIMA and CDIMA to date in the literature is roughly 1.5 times the smallest wavelength. In this Letter, we study the effect of halide salt addition on the wavelength of Turing patterns in CDIMA. Our experimental results give unprecedented, multifold increases in wavelength. We support these results with numerical simulations.

The patterns in this study were formed by the CDIMA reaction in the gel layer of a continuously fed unstirred tank reactor (CFUR) coupled with a continuously stirred tank reactor (CSTR) imaged by a CCD camera (PixeLINK). To determine the wavelength, an adaptive threshold filter is applied to the pattern. A 2D Fourier transform then is obtained for that image. Figure 1 illustrates the procedure from the Fourier transform. The averaged radial power ($\bar{P}$) is calculated by summing the intensity of the Fourier spectrum at a given radius and dividing by the number of points at that radius. The radius of the peak with the largest ($\bar{P}$) is then converted from a wave number to a wavelength.

Solutions were prepared to give concentrations of $[I_2] = 0.35$ mM, $[MA] = 1$ mM, $[ClO_2] = 0.1$ mM, $[\mathrm{poly(vinyl\,alcohol)}] = 10\ \mathrm{g\,L^{-1}}$, and $[H_2SO_4] = 10$ mM upon initial mixing in the reactor. Solutions were prepared as follows: I_2 was added along with H_2SO_4 and cosolvent acetic acid (10% v/v) and left to dissolve overnight. ClO_2

 © 2016 American Physical Society

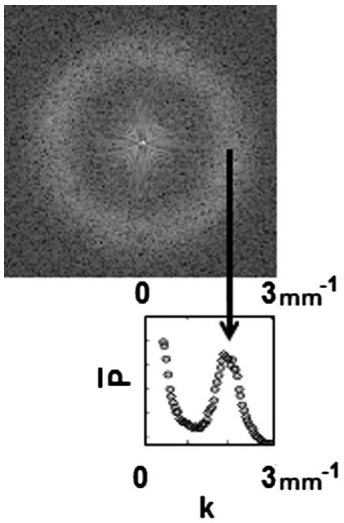

FIG. 1. Method of determining wavelength from Fourier transform of CDIMA pattern. Averaged radial power ($\bar{P}$) is determined from the sum of Fourier intensity at a given radius divided by the number of points at that radius. The wavelength determined for this pattern is the reciprocal of the wave number of the peak indicated by the arrow.

solution was prepared from stock that had been synthesized according to Ref. [20]. These solutions were kept in darkness after preparation to minimize photodegredation, and their concentrations were checked spectrophotometrically before each experiment. The poly(vinyl alcohol) (PVA, Sigma-Aldrich, average molecular weight 9000–10 000, 80% hydrolyzed) stock solutions and solutions of NaBr and NaCl were prepared freshly each week, while fresh NaI solutions were prepared immediately before each reaction run.

Solutions were fed via syringe pumps (New Era Pump Systems, NE-1600 and Cole-Palmer) into the CSTR, where they were mixed with three magnetic stirbars rotating at 1000 RPM. The CSTR chamber volume was 2.0 mL, and the residence time was 160 s. Quasi-two-dimensional patterns formed in the gel layer of the CFUR, which was composed of 2% agarose (Sigma-Aldrich, low EEO) gel with thickness less than the wavelength of the smallest pattern (maximum thickness 0.45 mm). Two membranes separated the CFUR and CSTR: a supported Anopore membrane (Whatman, pore size 0.2 μm, thickness 0.10 mm) impregnated with agarose gel (typically 4%) and a nitrocellulose membrane (Whatman, pore size 0.45 μm, thickness 0.12 mm). These membranes prevented advection in and provided support for the gel layer; the nitrocellulose also provided contrast for imaging. The working area of the reactor had a diameter of 25 mm. A glass optical window allowed for imaging of the patterns. This combined CFUR and CSTR reactor was thermostated at 4 °C.

Turing patterns began to appear spontaneously in the CFUR upon introduction of the ClO_2, I_2, and malonic acid solutions. The pattern morphologies were a mixture of spots and stripes with some honeycomb structures. Pattern wavelengths without halide addition were 0.51 ± 0.05 mm as determined from the Fourier transform. The halide flow rate was changed to vary the halide concentration in the reactor, and a fixed total flow rate and constant residence time were maintained by varying the flow rate of a feed of 10 mM H_2SO_4. Halide concentrations were increased stepwise.

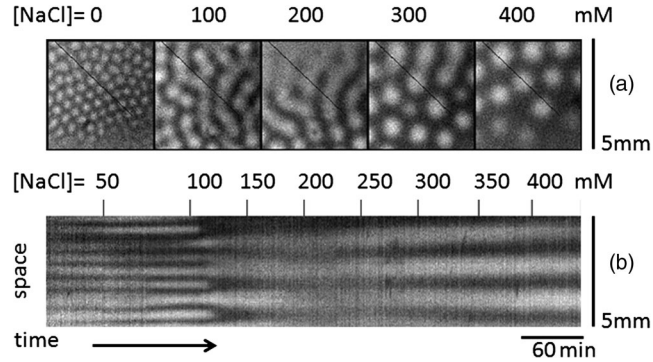

FIG. 2. Response of Turing patterns in the CDIMA system to addition of NaCl. Light and dark regions correspond to low and high PVA-triiodide complex concentrations, respectively. (a) Images showing response of initial pattern to concentrations of up to 400 mM NaCl. Image size is 5×5 mm. Slices from the black line in the figure are used to construct the space-time plot in (b). (b) Space-time plot [from the diagonal line in (a)] shows how the pattern transitions as the NaCl concentration is increased.

We present our results for Turing patterns subjected to the addition of sodium salts of bromide, chloride, and iodide through the feedstock. Figures 2 and 3 show the response of the native Turing patterns to the addition of NaCl and NaBr. Different transitions—wavelength doubling for the NaCl additions and pattern disappearance and regrowth for the NaBr additions—were observed in the corresponding space-time plots. The focus of this Letter is

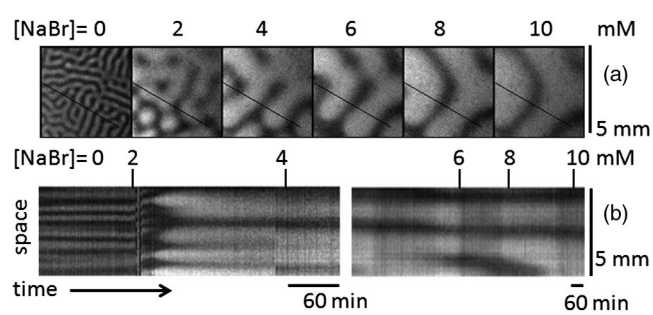

FIG. 3. Response of Turing patterns in the CDIMA system to addition of NaBr. Light and dark regions correspond to low and high PVA-triiodide complex concentrations, respectively. (a) Images showing response of initial pattern to concentrations of up to 10 mM NaBr. Image size is 5×5 mm. Slices from the black line in the figure are used to construct the space-time plot in (b). (b) Space-time plot [from the diagonal line in (a)] shows how the pattern transitions as the NaBr concentration is increased.

the occurrence of large wavelength patterns, but we find this dynamical aspect to be of interest and aim to do a more thorough investigation of these pattern transitions in the future.

In contrast to the changes observed with the addition of NaCl and NaBr, addition of NaI had nearly negligible effect on the pattern. Only sub-mM concentrations of NaI could be added to the reactor before the pattern was lost and a uniform steady state became stable. Additions of NaBr gave a uniform state at a higher threshold and with NaCl at an even higher threshold, in accordance with periodic trends. NaBr also had a more pronounced effect on the wavelength than NaCl. Figure 4 shows the concentration ranges where NaCl, NaBr, and NaI gave increases in pattern wavelength. Also shown in this figure are the largest patterns achieved by addition of each halide.

We used the following two variable model to simulate large changes in the pattern wavelength,

$$\partial u/\partial \tau = \frac{1}{s}\left(a - u - \frac{4u}{1+u^2}v + \nabla^2 u\right) \tag{1}$$

$$\partial v/\partial \tau = b\left(u - \frac{u}{1+u^2}v\right) - cv + d\nabla^2 v. \tag{2}$$

In this model, u is the dimensionless concentration of the activator species, iodide (I^-), and v is the dimensionless concentration of the inhibitor species, chlorite (ClO_2^-). The parameter s characterizes the triiodide-PVA complexation, and a and b are constants determined from the input concentrations of the reactants, which determine the kinetics of the reaction. The parameter d is the ratio of the diffusion constants for the two species: $d = D_{ClO_2^-}/D_{I^-}$.

The chlorite-iodide reaction step is first order in v and is accounted for in the third term of Eq. (1) and the second term of Eq. (2). We represent the chlorite-bromide and chlorite-chloride reactions with the $-cv$ term. This term is used to simplify the detailed kinetics of the bromide-related [21–24,24] and chloride-related [25–29] mechanisms into a reaction rate law that is first order in v and first order in halide concentration. Since in our study we use a large excess of bromide and chloride compared to chlorite, we further simplify the expression to a pseudofirst order form. The parameter c then reflects the nondimensionalized rate constant of the reaction and the concentration of halide added. When $c = 0$, this model reduces to the commonly used two-variable Lengyel-Epstein (LE) model [30].

The introduction of bromide and chloride into the system leads to the formation of the series of interhalogen compounds $I_3^- \leftrightharpoons I_2X^- \leftrightharpoons IX_2^- \leftrightharpoons X_3^-$ with the intermediates I_2, IX, X_2, where X is a bromine or chlorine atom [31–33]. The dihalogen species I_2 and Br_2 have been observed to affect the diffusion of their halide ions through the formation of the trihalide complexes. The triiodide complex slows the diffusion of iodide [34], and formation of the tribromide complex affects pattern stability in the Belousov-Zhabotinsky-aerosol OT pattern-forming system [35]. The equilibrium constants for the reaction of iodide with the diatomic interhalogens IBr and ICl are 4 and 8 orders of magnitude greater than that of the reaction of iodide with I_2, respectively [33]; thus, we propose IBr and ICl also affect the effective diffusion of iodide. We incorporate this effect

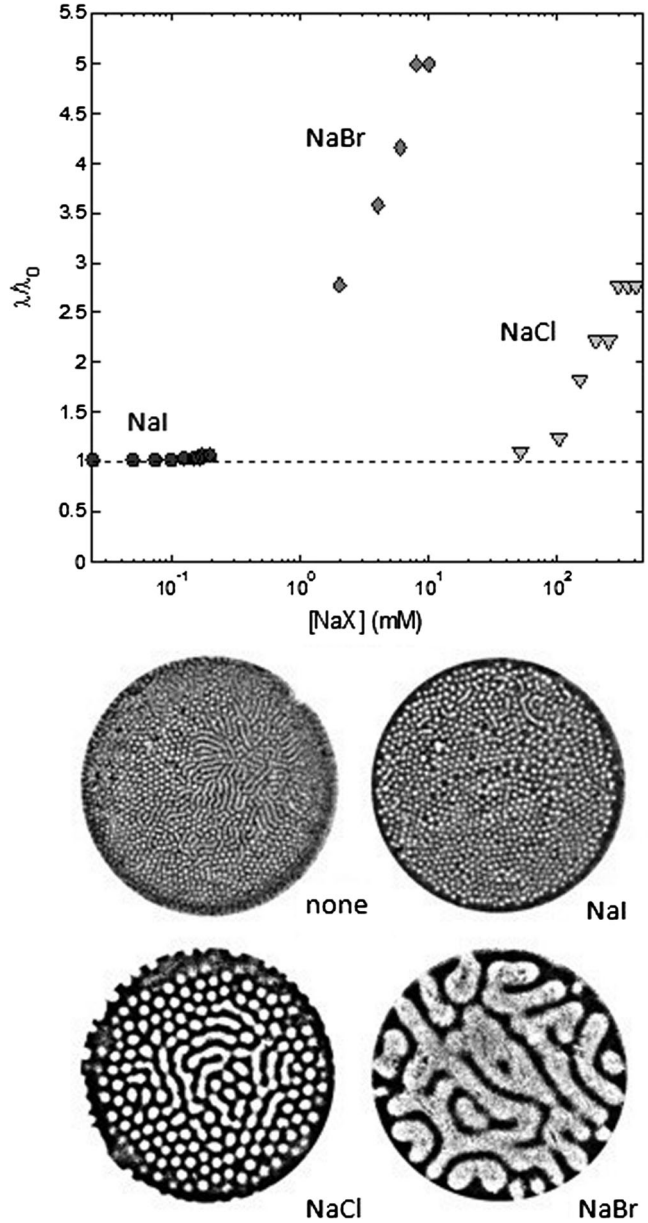

FIG. 4. Wavelengths of Turing patterns in the CDIMA reaction-diffusion system are altered by additions of sodium halides. (a) Semilog plot shows the ratio of wavelengths obtained at a given sodium halide feed concentration λ and at the original pattern wavelength λ_0. (b) The Turing patterns corresponding to the largest wavelength patterns shown in the plot are displayed. To compare all on the same scale, these images have been processed with an adaptive threshold filter. Reactor is 25 mm in diameter.

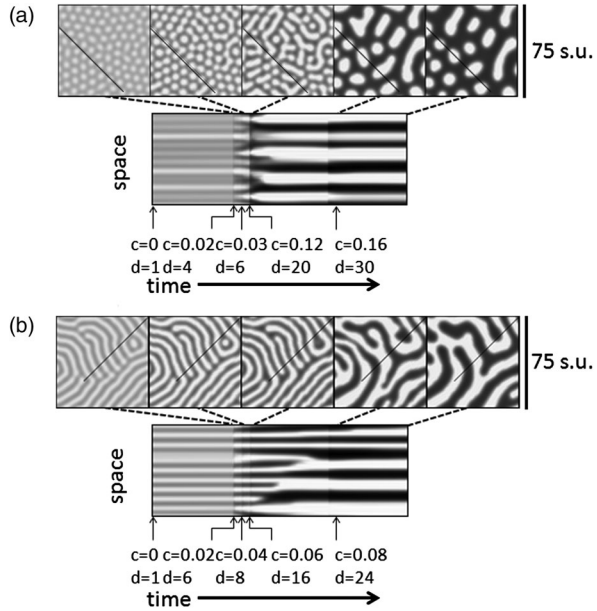

FIG. 5. Simulations with Eqs. (1) and (2) with a simultaneous increase in c and d. Stable Turing patterns are formed in the model with parameters $d = 1$, $a = 12$; $s = 20$; $c = 0$; $b = 0.36$ (a) and $b = 0.30$ (b). At the times indicated by the arrows, c and d are increased. Image sizes are 75×75 space units. (a) Space-time plot for transitions from a spot pattern with a (c, d) of (0, 1) to (0.02, 4) to (0.03, 6) to (0.12, 20) to (0.16, 30) shown with selected images immediately prior to transitions at $t = 5000$, 5100, 5200, 6200 with the last image at 7200 time units. (b) Space-time plot for transitions from a stripe pattern with a (c, d) of (0, 1) to (0.02, 6) to (0.04, 8) to (0.06, 16) to (0.08, 24) shown with selected images immediately prior to transitions at $t = 5000$, 5100, 5200, 6200 with the last image at 7200 time units.

into the model by changing the relative diffusion constant, d, increasing it as the effective diffusion constant of iodide decreases.

Neither chlorite consumption nor altered diffusion alone was sufficient to qualitatively reproduce the observed experimental patterns. A decrease in effective iodide diffusion caused the pattern morphology to change from spots and stripes to honeycomb patterns. Spot patterns could not be accessed after honeycomb ones simply by increasing d. Including only the loss of chlorite failed to change the spot and stripe widths significantly. With the inclusion of both effects, however, simulations were able to qualitatively reproduce an increase in pattern wavelength for stripes and spots (Fig. 5). Also, as observed in the experiments, we observed a loss of pattern above a certain threshold of the parameter c.

The main result that we present in this paper is the experimental observation of large increases in Turing pattern wavelength. This is the first report in a chemical system where a pattern's intrinsic wavelength has been increased by more than a factor of 2. The bromide addition results in a wavelength increase up to a factor of 5. This development enables a new avenue for research on pattern to pattern transitions in CDIMA without relying on spatial forcing. We are able to qualitatively reproduce these results by accounting for the effects that halide addition has on the kinetics of the reaction and the diffusion constants. Since CDIMA is the prototypical system for studying Turing pattern formation in reaction-diffusion systems, the potential impact of the study of pattern to pattern transitions in CDIMA is the development of insights for Turing pattern transitions in other systems. A deeper understanding of pattern to pattern transitions within the context of biomass patterns in arid ecosystems and those prone to fragmentation could lead to effective warning and management strategies for desertification and habitat fragmentation [8,10].

Another area where changes in pattern wavelength would be of interest is the evolution of patterns on animal skin. It has been proposed that zebra stripes are an evolutionary advantage in the presence of biting flies, as the flies have preferences for certain wavelengths of stripes over others [12]. There is also evidence that natural selection determines the spot wavelength in guppies [11], and such wavelength selection may be a general phenomenon.

We acknowledge funding from the following NSF sources: Grants No. DMR 0820492, No. CHE 1362477, and Graduate Research Fellowship No. 1102935.We thank Aric Hagberg and Ehud Meron for conversations on dynamics. We also thank Tamás Bánsági, Viktor Horváth, and Kenneth Kustin for their chemical knowledge and advice. Francisco Mello, our machinist, also deserves acknowledgment for his skill in helping us retool our systems and fabricate our reactor.

[1] T. Sekimura, C. Venkataraman, and A. Madzvamuse, PLoS One **10**, e0141434 (2015).
[2] M. Yamaguchi, E. Yoshimoto, and S. Kondo, Proc. Natl. Acad. Sci. U.S.A. **104**, 4790 (2007).
[3] D. Bullara and Y. De Decker, Nat. Commun. **6**, 6971 (2015).
[4] R. Sheth, L. Marcon, M. F. Bastida, M. Junco, L. Quintana, R. Dahn, M. Kmita, J. Sharpe, and M. A. Ros, Science **338**, 1476 (2012).
[5] R. HillerisLambers, M. Rietkerk, F. van den Bosch, H. Prins, and H. de Kroon, Ecology **82**, 50 (2001).
[6] E. Meron, E. Gilad, J. von Hardenberg, M. Shachak, and Y. Zarmi, Chaos Solitons Fractals **19**, 367 (2004).
[7] M. Scheffer, J. Bascompte, W. A. Brock, V. Brovkin, S. R. Carpenter, V. Dakos, H. Held, E. H. van Nes, M. Rietkerk, and G. Sugihara, Nature (London) **461**, 53 (2009).
[8] K. Siteur, E. Siero, M. B. Eppinga, J. D. M. Rademacher, A. Doelman, and M. Rietkerk, Ecol. Complex. **20**, 81 (2014).
[9] W. F. Laurance, H. E. M. Nascimento, S. G. Laurance, A. Andrade, R. M. Ewers, K. E. Harms, R. C. C. Luizão, and J. E. Ribeiro, PLoS One **2**, e1017 (2007).
[10] Á. de Frutos, T. Navarro, Y. Pueyo, and C. L. Alados, PLoS One **10**, e0118837 (2015).

[11] J. A. Endler, Evolution (Lawrence, Kans.) **34**, 76 (1980).
[12] T. Caro, A. Izzo, R. C. Reiner, H. Walker, and T. Stankowich, Nat. Commun. **5**, 3535 (2014).
[13] I. Lengyel, S. Kádár, and I. R. Epstein, Science **259**, 493 (1993).
[14] V. Castets, E. Dulos, J. Boissonade, and P. De Kepper, Phys. Rev. Lett. **64**, 2953 (1990).
[15] D. Feldman, R. Nagao, T. Bánsági, I. R. Epstein, and M. Dolnik, Phys. Chem. Chem. Phys. **14**, 6577 (2012).
[16] B. Rudovics, E. Barillot, P. W. Davies, E. Dulos, J. Boissonade, and P. De Kepper, J. Phys. Chem. A **103**, 1790 (1999).
[17] Z. Noszticzius, Q. Ouyang, W. D. McCormick, and H. L. Swinney, J. Phys. Chem. **96**, 6302 (1992).
[18] Q. Ouyang, R. Li, G. Li, and H. L. Swinney, J. Chem. Phys. **102**, 2551 (1995).
[19] D. G. Míguez, M. Dolnik, A. P. Muñuzuri, and L. Kramer, Phys. Rev. Lett. **96**, 048304 (2006).
[20] *Handbook of Preparative Inorganic Chemistry*, edited by G. Brauer (Academic Press, New York, 1963), 2nd ed.
[21] O. Valdes-Aguilera, D. W. Boyd, I. R. Epstein, and K. Kustin, J. Phys. Chem. **90**, 6702 (1986).
[22] R. H. Simoyi, J. Phys. Chem. **89**, 3570 (1985).
[23] M. Alamgir and I. R. Epstein, J. Phys. Chem. **89**, 3611 (1985).
[24] Z. Tóth and I. Fábián, Inorg. Chem. **39**, 4608 (2000).
[25] C. C. Hong and W. H. Rapson, Can. J. Chem. **46**, 2061 (1968).
[26] G. Schmitz and H. Rooze, Can. J. Chem. **65**, 497 (1987).
[27] G. Schmitz and H. Rooze, Can. J. Chem. **62**, 2231 (1984).
[28] J. S. Nicoson and D. W. Margerum, Inorg. Chem. **41**, 342 (2002).
[29] B. Kormányos, I. Nagypál, G. Peintler, and A. K. Horváth, Inorg. Chem. **47**, 7914 (2008).
[30] I. Lengyel and I. R. Epstein, Science **251**, 650 (1991).
[31] J. S. McIndoe and D. G. Tuck, Dalton Trans. **2003**, 244 (2003).
[32] L. F. Olsson, Inorg. Chem. **24**, 1398 (1985).
[33] R. C. Troy, M. D. Kelley, J. C. Nagy, and D. W. Margerum, Inorg. Chem. **30**, 4838 (1991).
[34] D. G. Leaist, J. Solution Chem. **17**, 359 (1988).
[35] V. K. Vanag and I. R. Epstein, Phys. Chem. Chem. Phys. **11**, 897 (2009).